Hydrol. Earth Syst. Sci. Discuss., 9, 7507–7541, 2012
www.hydrol-earth-syst-sci-discuss.net/9/7507/2012/
doi:10.5194/hessd-9-7507-2012

Hydrology and Earth System Sciences Discussions

Ice volume distribution and implications on runoff projections in a glacierized catchment

J. Gabbi[1], D. Farinotti[1], A. Bauder[1], and H. Maurer[2]

[1]Laboratory of Hydraulics, Hydrology and Glaciology (VAW), ETH Zurich, Gloriastrasse 37/39, 8092 Zurich, Switzerland
[2]Institute of Geophysics, ETH Zurich, Sonneggstrasse 5, 8092 Zurich, Switzerland

Received: 15 May 2012 – Accepted: 27 May 2012 – Published: 13 June 2012

Correspondence to: J. Gabbi (gabbij@vaw.baug.ethz.ch)

Published by Copernicus Publications on behalf of the European Geosciences Union.

Abstract

A dense network of helicopter-based ground penetrating radar (GPR) measurements was used to determine the ice-thickness distribution in the Mauvoisin region. The comprehensive set of ice-thickness measurements was combined with an ice-thickness estimation approach for an accurate determination of the bedrock. A total ice volume of $3.69 \pm 0.11\,km^3$ and a maximum ice-thickness of 290 m were found. The ice-thickness values were then employed as input for a combined glacio-hydrological model forced by most recent regional climate scenarios. This model provided glacier evolution and runoff projections. Runoff projections of the measured initial ice volume distribution show an increase in annual runoff of 4 % in the next two decades, followed by a persistent runoff decrease until 2100. Finally, we checked the influence of the ice thickness distribution on runoff projections. Our analyses revealed that reliable estimates of the ice volume is essential. Wrong estimations of the total ice volume might even lead to deviations of the predicted general runoff trend.

1 Introduction

The demand for renewable energy is rising, especially when considering the declining confidence in nuclear power and the ascending greenhouse gas emissions (BFE, 2011a). Particularly in alpine regions with sufficient amounts of precipitation, hydropower is one of the most efficient and appropriate energy sources (BFE, 2011b). In many high alpine basins the water supply to hydropower reservoirs primarily consists of melt water providing considerable amounts of water even in summer, when precipitation events are rare (Singh and Kumar, 1997; Bradley, 2006). Glaciers act as large freshwater reservoirs accumulating snow during the cold season and releasing the accumulated snow and ice as melt in summer. This leads to sustainable differences in the runoff regime of glacierized basins compared to a non-glacierized (Singh and Kumar, 1997). However, the projected climate change and the associated glacier retreat entail

HESSD
9, 7507–7541, 2012

the potential risk of serious diminution of the glacial induced water supply (Braun et al., 2000; Huss et al., 2008; Farinotti et al., 2011).

In recent years, different studies examined the impact of climate change on runoff projections for high-alpine basins (Bergström, 1995; Braun et al., 1995; Singh and Kumar, 1997; Braun et al., 2000; Schaefli, 2005; Huss et al., 2008; Farinotti et al., 2011). Highly glacierized catchments require appropriate modelling of glacial processes including mass balance modelling (Klok and Oerlemans, 2002; Pellicciotti et al., 2005; Huss et al., 2008) and adaptation of the glacier surface geometry (Vieli et al., 1997; Schneeberger et al., 2003; Huss et al., 2010; Jouvet et al., 2011). The initial ice volume distribution forms the basis for the determination of the glacier and runoff evolution of glacierized catchments. In order to deal with difficulties arising from the scarce or no data availability of the glacier bed, ice-thickness estimation approaches (e.g. Farinotti et al. 2009b; Fischer 2009; Paul and Linsbauer 2012) have been developped.

This study focuses on the determination of the glacier bed topography in the Mauvoisin region and the impact of the initial ice volume distribution on runoff projections of high-mountainous catchments. A dense network of helicopter- and ground-based ground penetrating radar (GPR) measurements served as data basis for the determination of the ice-thickness distribution. The ice-thickness measurements were combined with an ice-thickness estimation approach in order to determine the glacier bed topography in the study area as accurately as possible (Chapter 3). Integrating the newly acquired knowledge about the ice volume distribution, the Glacier Evolution and Runoff Model (GERM, Huss et al. 2008, Farinotti et al. 2011) forced by most recent climate scenarios (Bosshard et al., 2011) was applied to derive glacier evolution and runoff projections until 2100 for the region (Chapter 4). The model approach and the sensitivity of the model parameters have been tested in the study of Farinotti et al. (2011). In the scope of this study, the impact of inaccurate ice-thickness estimations, due to a lack of ice-thickness measurements or the usage of inappropriate ice-thickness estimation methods, on projections was analysed (Chapter 5). Uniform ice-thickness distribution, commonly used in macro-scale hydrological models, and more sophisticated results obtained from an ice-thickness estimation method (Farinotti et al., 2009b) deriving the distribution according to the surface topography were considered. Furthermore, the effect of over- or underestimation of the total ice volume was investigated.

2 Study site and data

The Mauvoisin area is situated in the south-western part of the Valais Alps, Switzerland (Fig. 1). The catchment extends over an area of 150 km^2, with 63 km^2 covered by glaciers in 2009, accommodating five larger glaciers (5–18 km^2) and several smaller glaciers (<5 km^2). A total ice volume of 3.69 ± 0.11 km^3 (2009) is determined for the region. 64 % of the total ice mass is stored in the two largest glaciers, Glacier de Corbassière and Glacier d'Otemma, covering an area of 18 and 16 km^2, respectively (Table 1). Due to the northwest orientation of the valley axis, the glaciers show exposures from southwest via north to east. They range in altitude from 2200 to 4300 m a.s.l. The local climate is characterized by mean precipitation amounts of about 1600 mm a^{-1} and a mean annual temperature of −3.5 °C.

The transient modelling of glacier and runoff evolution in the past and future requires a wide range of different data sets. Past temperature and precipitation time series as well as projections for the future climate are used to force the model (see Sect. 4.1.1). Direct mass balance measurements, decadal ice volume changes derived from topographic maps and areal photographs as well as runoff measurements are used for model calibration (Table 2). Due to long-term efforts, annual mass balance measurements are available since 1966 for Glacier du Giétro and since 1996 for Glacier de Corbassière (Bauder, 2003; Bauder et al., 2007). Digital elevation models (DEMs) of the glacier surface are available for the years 1934, 1983 and 2009 for all glaciers in the catchment. Additional DEMs of the years 1997/1998 and 2003 exist for Glacier de Corbassière and Glacier du Giétro, respectively. DEMs of the year 1934 are based on topographic maps whereas the others are derived by areal photographs. More details about the data base are shown in Table 2.

HESSD
9, 7507–7541, 2012

Runoff data are available from the hydropower company Mauvoisin since the beginning of the 1980s. The data includes water level variations of the Mauvoisin reservoir and the input of the water conducting pipeline in the west (Fig. 1). Runoff measurements have monthly resolution for the period 1982 to 2000 and daily resolution since 2000. According to the available runoff data, we divided the basin into two subcatchments, the *Mauvoisin catchment* which correspond to the natural catchment of the reservoir and the *Corbassière/Petit Combin catchment* which represents the area in the west including Glacier de Corbassière and Glacier du Petit Combin (Fig. 1).

3 Ice-thickness distribution

3.1 GPR measurements

In spring 2011, helicopter-based GPR surveys were carried out on the five largest glaciers in the Mauvoisin region (see Table 2). 122 km of GPR profiles were recorded whereof 55 % showed significant bedrock reflections, such that they could be incorporated in the ice volume calculation. The data were acquired by the commercial company *Radar Systemtechnik RST GmbH* (Salem, Germany). They employed an acquisition unit operating in a gated stepped mode using frequencies between 50 and 150 MHz (RST, 2012). Additionally, ground-based GPR measurements from previous field campaigns of the years 1988/1998 and 1997 on Glacier de Corbassière and Glacier du Giétro, respectively, were included (Fig. 3, VAW 1998).

3.1.1 GPR processing

Visualization of the bedrock topography in the GPR sections required several processing steps to be applied. The helicopter-borne GPR data were acquired more or less continuously during the flights. In a first step, straight profile traces needed to be identified on which the positions of the individual GPR signals were projected. Then, spatial filters were applied to remove the inherent system ringing of GPR acquisition systems.

HESSD
9, 7507–7541, 2012

In a next step, a bandpass filter was applied, which removed signal portions outside of the frequency band radiated by the GPR transmitter antenna. Then, the reflected signals from the glacier surface had to be identified in the GPR sections, which allowed static corrections to be applied. A further critical processing step included application of gain functions for enhancing small amplitudes at later times in the radargrams (e.g. bedrock reflections). The signal-to-noise ratio was further improved by defining discrete bins along the profiles and stacking the traces contained in each bin. Finally, a Kirchhoff Migration was applied for removing artefacts produced by point scatterers (e.g. large boulders) and to correctly position the reflectors in the individual sections. Figure 2 shows a finally processed section across the Glacier d'Otemma. The bedrock reflection is clearly visible and reaches its maximum depth of about 250 m at a horizontal distance of 550 m.

3.2 Ice-thickness estimation

Since the GPR profiles covered only a relatively small portion of the glacierized area, an extrapolation procedure was required for obtaining estimates over the entire area of interest. The literature includes different ice-thickness estimation approaches of various complexity (e.g. Farinotti et al. 2009b; Fischer 2009; Paul and Linsbauer 2012). All of them combine ice flow mechanics with the information about the surface topography for estimating the depth of the glacier bed.

In this study we considered the Ice-Thickness Estimation Method (ITEM) of Farinotti et al. (2009b). ITEM derives the ice-thickness distribution by calculating the ice flow and ensuring mass continuity. Two gradients for the so called apparent mass balance (i.e. the difference between the actual mass balance and the rate of ice-thickness change), one for the ablation and one for the accumulation zone, have to be assumed. The ice flow is converted into ice-thicknesses by inversion of Glen's flow law (Glen, 1955). A correction factor c accounts for the valley shape, basal sliding and uncertainties in the chosen flow parameters. This factor has to be calibrated by ice-thickness measurements or estimated from other glaciers.

We have considered our GPR measurements for identifying suitable calibration factors for each profile. In between the profiles, the calibration factors were linearly interpolated. On glaciers, where no GPR data were available, a mean correction factor was used. Gradients of the apparent mass balance were derived by the results of the mass balance model and the observed ice-thickness changes (Table 4).

3.3 Results

Based on all available ice-thickness measurements a total ice volume of $3.69 \pm 0.11\,\mathrm{km}^3$ was determined for the Mauvoisin region for the year 2009 (Fig. 3). Glacier de Corbassière is the largest glacier in the area with an ice volume of $1.38 \pm 0.07\,\mathrm{km}^3$. Glacier d'Otemma shows a slightly smaller ice volume of $1.05 \pm 0.05\,\mathrm{km}^3$. The three other larger glaciers, Glacier du Brenay, Glacier du Mont Durand and Glacier du Giétro, have clearly lower ice volumes ranging between 0.30 ± 0.02 and $0.45 \pm 0.02\,\mathrm{km}^3$ (Table 1). All smaller glaciers together account for $0.13 \pm 0.05\,\mathrm{km}^2$ corresponding to approximately 4 % of the total ice volume. The largest ice thickness (291 m) was found on Glacier d'Otemma. The maximum ice thickness of Glacier de Corbassière is 238 m. Glacier du Brenay and Glacier du Giétro have maximal ice-thicknesses around 220 m. In comparison, Glacier du Mont Durand shows a lower maximal ice-thickness of only 144 m (Table 4).

4 Glacier evolution and runoff modelling

4.1 Glacio-hydrological model

For glacier and runoff projections the glacio-hydrological model GERM was applied (Huss et al., 2008; Farinotti et al., 2011). The model is fully distributed and consists of five different modules dealing with accumulation and ablation processes, glacier evolution, evaporation and runoff routing. Model and applications on alpine catchments are described in Huss et al. (2008) and Farinotti et al. (2011).

HESSD
9, 7507–7541, 2012

4.1.1 Model forcing

The model is forced with continuous temperature and precipitation time series. In order to reconstruct the past climate conditions in Mauvoisin area, regional temperature and precipitation data from weather stations in the vicinity of the study site are taken into account. For the past temperature evolution the homogenized climate data of the weather station in Sion is used (Begert et al., 2005). In order to determine a local temperature lapse rate weather stations closer than 50 km to the study area are considered (Fig. 1). Precipitation time series for the Mauvoisin region are computed on the basis of three weather stations (Bourg-St-Pierre, Sion, Bern) and from the PRISM data set (Schwarb et al., 2001; Huss et al., 2008).

Future climate time series of the Mauvoisin region are based on scenarios developed in the framework of the European ENSEMBLES project (van der Linden and Mitchell, 2009). Regional climate scenarios of 10 different model chains based on emission scenario SRES A1B (IPCC, 2000) were used. The data were obtained from the *Center for Climate Systems Modeling (C2SM)* providing daily temperature and precipitation changes for two periods in the future in comparison to a period in the past (CH2011, 2011; Bosshard et al., 2011).

In order to meet the model requirements of continuous climate time series the differences in temperature and precipitation between the different periods are linearly interpolated and an interannual variability based on the past is introduced. We followed the approach of Farinotti et al. (2011) and generated 100 different time series.

4.1.2 Calibration

The calibration of the model parameters was performed as described in Huss et al. (2008) and Farinotti et al. (2011). In a first step, the parameters of the melt and the accumulation module are calibrated for reproducing the measured ice volume changes (Huss et al., 2008). In a second step, the parameters of the runoff model are adapted. For validation the measured and simulated daily, monthly and annual runoff volumes

HESSD
9, 7507–7541, 2012

are compared and the Nash-Sutcliffe criterion was calculated (Nash and Sutcliffe, 1970). The Nash-Sutcliffe criterion lies in a range of 0.93–0.94 for monthly and between 0.79–0.85 for daily runoff values. The parameters of the evaporation module are adopted from Huss et al. (2008) and Farinotti et al. (2011).

4.2 Glacier evolution

Since the beginning of the 20th century, the glaciers in the Mauvoisin region have been in retreat. Between 1900 and 2009 the initial ice volume has decreased by 43 %, from 6.49 km^3 to 3.69 km^3. Almost half of this ice volume loss occurred during the past 30 years. Hence, the retreat rate has nearly doubled since the beginning of the 1980s (Fig. 4). Similar mass balance rates could be also observed between 1943 and 1954. Only a short period of mass gain was observed between 1978 and 1983, when the ice volume increased by about 192 mio m^3 corresponding to an increase of 3.6 % in total ice masses.

Independently of the size, all glaciers in the Mauvoisin region will severely retreat in the future. By the end of the 21st century, the entire area will be nearly ice free. Only some ice patches above 3500 m a.s.l., with a total ice volume of 0.11 km^3 (0.08 $\leftrightarrow$ 0.24 km^3), are expected to remain. Small glaciers will vanish completely.

The amount of retreat of the glaciers in the Mauvoisin region is mainly controlled by the elevation of their accumulation area (Fig. 5). Small glaciers or parts of them below 3000 m a.s.l. will disappear by 2020 as in the case of Glacier de Fenêtre, Glacier de la Tsessette and, to some extent, also Glacier de Crête Sèche. Small glaciers situated at higher altitudes, such as Glacier de Tournelon Blanc, will persist.

The larger glaciers, especially those with large ice volumes and high-altitude accumulation areas, will retreat considerably slower than the smaller ones. Within the next few decades, the larger glaciers will be affected mainly by thinning. Only at a later stage (after 2050) the glaciers are expected to show significant areal wastage. Glacier d'Otemma shows a particularly fast retreat in contrast to the other larger glaciers in the area. Already around 2070 Glacier d'Otemma will have almost entirely vanished

HESSD
9, 7507–7541, 2012

except of some tiny ice patches in the uppermost part. The reason for the rapid retreat of the Glacier d'Otemma despite the large initial ice volume can be associated with its main basin restricted to altitudes below 3100 m a.s.l. In comparison, in 2070 Glacier de Corbassière will cover almost the half of its initial area because of considerable ice masses situated at altitudes above 4000 m a.s.l.

4.3 Hydrology

Between 1900 and 2009 the annual runoff increased from 216 to 265 mio $m^3 a^{-1}$ (23 %), but this rise was not constant over time. In two successive periods from 1910 to 1945 and from 1975 to 1995 the annual runoff volume has increased by about 45 mio $m^3 a^{-1}$ (~20 %) and has reached maximal runoff of approximately 260 mio $m^3 a^{-1}$. In between, the annual runoff volume dropped back to values of less than 220 mio $m^3 a^{-1}$. These fluctuations can be correlated with the glacier evolution as well as with changes in temperature and precipitation (Fig. 6). In the next two decades, annual runoff will augment to approximately 275 mio $m^3 a^{-1}$ (+4 %). Afterwards, a continuous decline is expected until the end of the 21st century. Compared to the maximal runoff volume of 275 mio $m^3 a^{-1}$ the annual runoff will drop about 25 % to 207 mio $m^3 a^{-1}$ until 2100.

The changing climate and the associated glacier wastage will not only affect the amount of annual runoff, but also the individual runoff components, leading to significant changes in the runoff regime. At present, the runoff regime is dominated by ice melt and shows a peak discharge in the months July and August (Fig. 7). In the future, mean daily runoff in summer will strongly diminish, whereas during winter daily runoff will slightly enhance due to higher air temperatures. Currently, a maximum mean daily runoff of 28 $m^3 s^{-1}$ is attained at the end of July, which will decrease to 18 $m^3 s^{-1}$ until the year 2100. Beside the reduction of daily runoff also a shift of peak runoff is expected. At the end of the 21st century maximal runoff values will occur one-and-a-half months earlier compared to the reference period. This shift of the peak discharge from end of July to the mid of June results from the decrease of the runoff volumes in the months July to September of about 44 % compared to the reference period. Furthermore, daily runoff will increase slightly earlier in spring compared to the present situation due to the earlier onset of the snow melt season. The time offset between the beginning of the melt season in the reference period and in 2100 is around three weeks.

The reason for these changes in runoff regime becomes evident by considering the evolution of the different runoff components with progressing climate change. The model employed distinguishes between: runoff originating from glacier, snow melt, non-glacierized areas and the subsurface. During the reference period, snow and glacier melt are the main components and account together for 66 % of the total runoff. Snow melt contribution starts to increase at the beginning of May and reaches a maximum at the beginning of July. The glacier melt increases later in the season and its maximum occurs around the beginning of August. These two runoff components explain the high runoff volume in the months July and August of the present runoff regime. For the next 20 to 30 yr, glacier melt remains at high level and accounts for about 25 % of the total runoff. In a subsequent period, glacier melt will decrease the contribution to total runoff to 5 % (Fig. 7).

Also the snow melt will experience a strong reduction, but it will be less pronounced than the ice melt. In the year 2100, the snow melt accounts for about 30 % of the total catchment runoff. The reason for this reduction in snow melt is primarily caused by less solid precipitation due to the expected temperature rise and secondarily by generally decreased precipitation. In fact, total precipitation will reduce about 6 % until 2100 compared to the reference period (1980–2009). In contrast, solid precipitation will suffer a decrease of about 33 % over the same period. In addition, snow melt peak is shifted from the beginning of July to the mid of May as a result of the earlier initiation of the snow melt season related to the warmer climate. The runoff of non-glacierized areas and the subsurface will not change significantly in the future. Until 2100 both runoff components will show a slight increase only, due to the area becoming glacier-free.

HESSD

9, 7507–7541, 2012

5 Ice volume sensitivity analysis

Extensive helicopter-borne GPR measurements allowed the ice thickness distribution in the Mauvoisin area to be delineated quite accurately. If such data sets are not available, simplified models need to be employed. By means of a sensitivity analysis we have quantified the influence of the initial ice thickness distribution on glacier and runoff projections.

For that purpose, we considered five different ice-thickness distribution estimation procedures:

1. Approach as described in Sect. 3.2. Case (1) refers to the reference ice-thickness distribution based on the measurements.

2. Same ice-thickness distribution pattern as (1) but scaled by +20 %. This case shows the influence of overestimated total ice volumes on runoff projections.

3. Same ice-thickness distribution pattern as (1) scaled by −20 %. Case (3) emphasizes the impact of underestimation of the total ice volume on the runoff evolution.

4. Uniform ice thickness distribution with a mean ice-thickness calculated by the ice volume based on (1) for each glacier. This distribution is the most simple case and is used in most marco-scale hydrological models where ice volume is crudely processed (Fig. 8d).

5. Ice-thickness distribution calculated by the ITEM assuming a correction factor c of 0.53 as used in the study by Farinotti et al. (2009a) for unmeasured glaciers. Apparent mass balance gradients are set to $0.9 \times 10^{-2}\ \mathrm{a}^{-1}$ for the ablation zone and to $0.5 \times 10^{-2}\ \mathrm{a}^{-1}$ for the accumulation zone. This method provides a spatial distribution pattern based on the glacier surface topography. Case (5) shows the performance of ITEM if no ice-thickness measurements are available (Fig. 8b).

When assuming a constant correction factor $c = 0.53$ (5), ITEM overestimates the total ice volume of the Mauvoisin region by about 36 % (Table 4). Especially, for Glacier

HESSD
9, 7507–7541, 2012

du Brenay and Glacier du Mont Durand the ice volume is overestimated by 61 and 80 %, respectively. Glacier du Giétro shows in case of $c = 0.53$ an exceptional small deviation of only −7 %. Glacier de Corbassière and Glacier d'Otemma show mainly in the lower area large ice-thickness deviations between the GPR and the ITEM based bed topography of up to 130 m (Figs. 8 and 9). Glacier du Brenay and Glacier du Mont Durand show deviations in ice-thickness of the same order, but the largest deviations are located more on the center than on the lower part of the glacier.

5.1 Impact of initial ice volume distribution on runoff

The different ice volumes an spatial ice-thickness distribution patterns significantly affect the runff projections. In case of the GPR derived ice volume (1) annual runoff will slightly increase about 4 % until around 2030 to a maximal annual runoff volume of 275 mio $m^3 a^{-1}$. Afterwards, the runoff volume starts to decrease gradually until 2100 (Fig. 6). Overestimation of the total ice volume of about 20 % (2) results in a pronounced increase of the annual runoff over a prolongated period of time compared to GPR derived runoff (Fig. 10). Peak discharge will occur around 10 yr later with a volume of 279 mio $m^3 a^{-1}$ (+1 %). Underestimation of the total ice volume (3) lead in the case of the Mauvoisin region to changes in the trend of the runoff evolution in the next decades. Instead, a further increase of runoff volumes, annual runoff continuously decreases until the end of the 21st century with general lower runoff volumes compared to GPR derived results. Neglecting a specific spatial ice volume distribution by assuming uniform ice thickness distribution (4) leads to an overestimation of the runoff in the next two decades due to too large ice masses in low altitude. Maximal annual runoff will occur around 2020 with a peak discharge of 283 mio $m^3 a^{-1}$ (3 %). In a later stage, the runoff of the uniform ice volume distribution align to the GPR derived runoff curve. The applications of ITEM with the uncalibrated and fixed parameter set (5) overestimates the ice volume in the Mauvoisin region about 36 % which results in a similar runoff evolution as in case of the ice volume overestimated by 20 % (2). But, in Case (5) the annual

HESSD
9, 7507–7541, 2012

runoff shows a sharper increase of 12 % until the beginning of 2040. A maximum peak runoff of 287 mio $m^3 a^{-1}$ is expected in this case.

6 Discussion

The ice volume sensitivity study emphasizes the importance of an accurate ice volume determination. The incorporation of ice-thickness measurements in the ice volume calculation is crucial in order to receive reliable ice volumes and thickness distributions. Inaccurate estimations of the total ice volume might entail deviations from the predicted general runoff trend. In case of the Mauvoisin region it could be shown that an overestimated ice volume reveals a sharp runoff increase in the the next few decades, whereas estimations supported by measurements show almost no further increase in annual runoff. The ice-thickness distribution affects the runoff evolution as well, but not as pronounced as in case of an overestimated ice volume. A uniform ice volume distribution entails particularly in the next few decades an overestimation of runoff and is therefore for projections not suitable. After major ice volume has melted it only differs slightly from the GPR derived runoff evolution. In absence of ice-thickness measurements a mean parameter set has to be assumed carrying the potential of over- or underestimation of the true ice volume. In case mass balance measurements are available, mass balance gradients can be adjusted leading to improvements in the ice volume estimation. Due to the high sensitivity of the correction factor on the ice volume estimation (Farinotti et al., 2009b), the usage of an appropriate correction factor is of much higher importance compared to the mass balance gradients. Knowledge about the local ice-thickness enables the calibration of the correction factor resulting in a significantly increased accruacy of the ice volume estimation. New approaches are required for better assessing correction factors for individual glaciers if no ice-thickness measurements are available. Our results suggest that the incorporation of GPR based ice-thickness measurements is of high importance in order to provide reliable runoff

HESSD
9, 7507–7541, 2012

projections especially for the next thirty to forty years when profound changes are expected.

Despite the high density of ice-thickness measurements and the application of an ice-thickness estimation method, the true geometry of the bed topography is not fully known. Uncertainties arise particularly on separated glacier branches or on single glaciers where no measurements are available.

The reliability and usefullness of the glacier evolution and runoff projections is also affected by uncertainties in the future climate evolution. The climate scenarios applied are based on the most recent climate study and incorporated different combinations of regional and general circulation models. However, only emission scenario SRES A1B (IPCC, 2007) was considered. Deviations from the chosen emission scenario might entail a different glacier evolution and consequently changes in the projected future runoff regime.

Uncertainties arise also from the chosen model approach. The prediction of the glacier evolution is determined on the basis of a temperature-index melt model in combination with an accumulation model. Due to the low data requirement of this approach, it is well suited for distributed modelling of entire catchments and available for future climate scenarios. But, temperature-index melt models act just as simplified approaches of the true surface energy balance and react only to changes in the temperature and precipitation field. Other factors, such as variations in incoming or outgoing radiation or changes in the wind field, are not incorporated and may lead to different results. In the 1940s, a rise in the global radiation led to higher melting rates compared with today's climate conditions despite of lower air temperatures (Huss et al., 2009). Such variations of solar radiation are not captured by temperature-index melt models retaining a constant parameter set and might yield discrepancies between projected and real glacier evolution.

Furthermore, uncertainties about the model parameters have the potential to cause deviations from glacier and runoff projections. The study of Farinotti et al. (2011) reveals that particularly the temperature gradient and the melt parameters are sensitive for runoff projections. The study shows that a reduction of the temperature lapse rate by 10 % yield a decrease of the mean annual runoff of about 25 % and that an increase of the melt parameters of 10 % lead to an increase of the mean annual runoff of 11 to 20 %. The temperature distribution has a big impact on runoff projections because it controls the snow and ice melt and additionally also the phase of precipitation. Under- or overestimation of the total ice volumes leads to deviations in the mean glacier melt of the same order. In case of the ITEM-derived glacier bed topography the total ice volume is overestimated by 36 % leading to a reduction of the mean glacier-induced runoff of about 31 %. This corresponds to a mean annual runoff reduction of about 4 %, what is less than the effect of the temperature gradient and the melt parameters, because the ice volume affects the ice melt component only. But, the discrepancy between the two runoff evolutions is higher for individual years, as around 2050, where the annual runoff based on the ITEM-derived ice volume distribution is overestimated by about 10 %.

Enlargement of debris covered area of a glacier might yield attenuation of the glacier retreat in future. Glacier d'Otemma and Glacier du Brenay show already an extended debris cover in the ablation zones. During the last decades, especially small glaciers in the Mauvoisin area have shown a strong increase in debris cover. Similar observations have been reported from other mountain regions (Kellerer-Pirklbauer, 2008; Popovnin and Rozova, 2002; Stokes et al., 2009). In contrast, an increase in dust cover reduces the albedo and lead to an intensification of the melt process (Oerlemans et al., 2009). Insufficient understanding of the processes yielding changes in debris or dust cover and lack of data inhibit the implementation of debris cover evolution in melt models (Reid and Brock, 2010).

Moreover, the glacier evolution also involves uncertainties arising from the accumulation model. The spatial distribution of precipitation and the distinction between liquid and solid precipitation is complex. Variable redistribution of snow by wind and avalanches increases the complexity of the accumulation further (Lehning et al., 2008). The applied model includes a simplified snow redistribution approach but assumes

HESSD
9, 7507–7541, 2012

Ice volume distribution and implications on runoff projections

J. Gabbi et al.

constant snow redistribution patterns in time. Further effort is required to increase the accuracy in modelling the snow distribution on glaciers (Dadic, 2008).

7 Conclusions

In this study we combined results from extensive GPR measurements with an ice thickness estimation approach (Farinotti et al., 2009), for determining the present ice volume in the Mauvoisin area. This served as input for a combined glacio-hydrological model (Huss et al., 2008; Farinotti et al., 2011), with which glacier and runoff projections could be determined. By means of a sensitivity analysis we could demonstrate that consideration of GPR data is critical and that overly simplified ice thickness models may lead to severe distortions of the runoff projections. A total ice volume of $3.69 \pm 0.11\,\mathrm{km}^3$ was calculated by including all available measurements and a maximal ice-thickness of 291 m was found.

In the next few decades the annual runoff will slightly rise to a maximum of $275\,\mathrm{mio\,m^3\,a^{-1}}$ around 2030. This period will be followed by a strong decrease of the annual runoff to volumes below present values by the end of the 21st century caused by decreasing glacier melt contribution. The runoff regime is also subjected to significant changes. Under present conditions, around 60 % of the annual runoff in the Mauvoisin catchment occurs during the months July and August, whereas by 2100 the runoff in July and August will be reduced by half. Peak discharge will occur one and a half month earlier by 2100 than in the reference period. Reasons for these changes can be found in the strong decline of the glacier melt supply, the decreasing snow melt contribution and the earlier intitiation of the snow melt season.

HESSD
9, 7507–7541, 2012

Acknowledgements. Our particular thanks go to the *Forces Motrices de Mauvoisin SA* which has enabled and supported different data acquisitions in the Mauvoisin region. They have also provided long-term measurement series of the inflow to the reservoir. Further, we thank the *Center for Climate Systems Modeling (C2SM)* which provided regional climate scenarios of FUGE project. Finally, we would like to acknowledge Bruno Nendela and Hermann Bösch for topographic and photogrammetrical analysis. This study is a contribution to NRP 61.

References

Bauder, A.: Automatic surveying for hazard prevention on Glacier de Giétro, in: Milestones in Physical Glaciology From the Pioneers to a Modern Science, 180, 1–3, Mitteilung der Versuchsanstalt für Wasserbau Hydrologie und Glaziologie, ETH Zürich, International Glaciological Symposium held in honor of Prof. Dr. Hans Röthlisberger on the occasion of his 80th birthday, 14 February 2003, 2003. 7510

Bauder, A., Funk, M., and Huss, M.: Ice volume changes of selected glaciers in the Swiss Alps since the end of the 19th century, Ann. Glaciol., 46, 145–149, 2007. 7510

Begert, M., Schlegel, T., and Krichhofer, W.: Homogeneous temperature and precipitation series of Switzerland from 1864 to 2000, International J. Climatol., 25, 65–80, 2005. 7514

Bergström, S.: The HBV model, in: Computer Models of Watershed Hydrology, edited by: Singh, V., Water Resources Publications: Highlands Range Colorado, USA, 443–476, 1995. 7509

BFE: Engergieperspektiven für die Schweiz bis 2050, Tech. rep., Departement für Umwelt, Verkehr, Energie und Kommunikation, Bundesamt für Energie, 2011a. 7508

BFE: Wasserkraft, Tech. rep., Departement für Umwelt, Verkehr, Energie und Kommunikation, Bundesamt für Energie, 2011b. 7508

Bosshard, T., Kotlarski, S., Ewen, T., and Schär, C.: Spectral representation of the annual cycle in the climate change signal, Hydrol. Earth Syst. Sci., 15, 2777–2788, doi:10.5194/hess-15-2777-2011, 2011. 7509, 7514

Bradley, R.: Threats to water supplies in the Tropical Andes, Science, 312, 1755–1756, 2006. 7508

Braun, L. N., Aellen, M., Funk, M., Hock, R., Rohrer, M. B., Steinegger, U., Kappenberger, G., and Müller-Lemans, H.: Measurements and simulations of high alpine water balance components in the Linth-Limmeren head watershed (north-eastern Switzerland), Zeitschrift für Gletscherkunde und Glazialgeologie, 30, 161–185, 1995. 7509

Braun, L. N., Weber, M., and Schulz, M.: Consequences of climate change for runoff from Alpine regions, Ann. Glaciol., 31, 19–25, 2000. 7509

CH2011: Swiss Climate Change Scenarios 2011, published by C2SM, MeteoSwiss, ETH, NCCR Climate, and OcCC, Zurich, Switzerland, 88 pp., 2011. 7514

Dadic, R.: Monitoring and modelling snow and accumulation processes in glacierized alpine basins, Ph.D. thesis, ETH-Zürich, Institute for Environmental Engineering (IfU), no. 17945, 2008. 7523

Farinotti, D., Huss, M., Bauder, A., and Funk, M.: An estimate of the glacier ice volume in the Swiss Alps, Global Planet. Change, 68, 225–231, doi:10.1016/j.gloplacha.2009.05.004, 2009a. 7518

Farinotti, D., Huss, M., Bauder, A., Funk, M., and Truffer, M.: A method to estimate ice volume and ice thickness distribution of alpine glaciers, J. Glaciol., 55, 422–430, 2009b. 7509, 7510, 7512, 7520

Farinotti, D., Usselmann, S., Huss, M., Bauder, A., and Funk, M.: The runoff evolution in the Swiss Alps: Projections for selected high-alpine catchments based on ENSEMBLES scenarios, Hydrol. Process., online first: doi:10.1002/hyp.8276, 2011. 7509, 7513, 7514, 7515, 7521

Fischer, A.: Calculation of glacier volume from sparse ice-thickness data, applied to Schaufelferner, Austria, J. Glaciol., 55, 453–460, 2009. 7509, 7512

Glen, J. W.: The creep of polycrystalline ice, Proc. R. Soc. Lon. Ser.-A, 228, 519–538, 1955. 7512

Huss, M., Farinotti, D., Bauder, A., and Funk, M.: Modelling runoff from highly glacierized alpine drainage basins in a changing climate, Hydrol. Process., 22, 3888–3902, doi:10.1002/hyp.7055, 2008. 7509, 7513, 7514, 7515

Huss, M., Funk, M., and Ohmura, A.: Strong Alpine glacier melt in the 1940s due to enhanced solar radiation, Geophys. Res. Lett., 36, L23501, doi:10.1029/2009GL040789, 2009. 7521

Huss, M., Jouvet, G., Farinotti, D., and Bauder, A.: Future high-mountain hydrology: a new parameterization of glacier retreat, Hydrol. Earth Syst. Sci., 14, 815–829, doi:10.5194/hess-14-815-2010, 2010. 7509

IPCC: IPCC Emission Scenarios (SRES), Nakicenovic N, Swart R (eds), Cambridge University Press, 570 pp., 2000. 7514

IPCC: Climate Change 2007. The Physical Scientific Basis. Contributions of Working Group I to the Fourth Assessment Report of the Intergovernmental Panel on Climate Change, Tech. rep., WMO/UNEP, Cambridge University Press, available at: http://www.ipcc.ch/publications_and_data/ar4/wg1/en/contents.html (last access: 11 June 2012), 2007. 7521

Jouvet, G., Hus, M., Funk, M., and Blatter, H.: Modelling the retreat of Grosser Aletschgletscher, Switzerland, in a changing climate, J. Glaciol., 57, 1033–1044, 2011. 7509

Kellerer-Pirklbauer, A.: The supraglacial debris system at the Pasterze Glacier, Austria: spatial distribution, characteristics and tranpsort of debris, Z. Geomorphol., 52, 3–25, 2008. 7522

Klok, E. J. and Oerlemans, J.: Model study of the spatial distribution of the energy and mass balance of Morteratschgletscher, Switzerland, J. Glaciol., 48, 505–518, 2002. 7509

Lehning, M., Loewe, H., Ryser, M., and Raderschall, N.: Inhomogeneous precipitation distribution and snow transport in steep terrain, Water Resour. Res., 44, W07404, doi:10.1029/2007WR006545, 2008. 7522

Nash, J. E. and Sutcliffe, I. V.: River flow forcasting through conceptual models Part I – A discussion of principles, J. Hydrol., 10, 282–290, 1970. 7515

Oerlemans, J., Giesen, R., and van den Broeken, M.: Retreating alpine glaciers: increased melt rates due to accumulation of dust (Vadret da Morteratsch, Switzerland), J. Glaciol., 55, 729–736, 2009. 7522

Paul, F. and Linsbauer, A.: Modeling of glacier bed topography from glacier outlines, central branch lines, and a DEM, Int. J. Geogr. Inf. Sci., online first: doi:10.1080/13658816.2011.627859, 1–18, 2012. 7509, 7512

Pellicciotti, F., Brock, B. J., Strasser, U., Burlando, P., Funk, M., and Corripio, J.: An enhanced temperature-index glacier melt model including the shortwave radiation balance: development and testing for Haut Glacier d'Arolla, Switzerland, J. Glaciol., 51, 573–587, 2005. 7509

Popovnin, V. and Rozova, A.: Influence of sub-debris thawing on ablation and runoff of the Djankuat Glacier in the Caucasus, Nord. Hydrol., 33, 75–94, 2002. 7522

Reid, T. and Brock, B.: An energy-balance model for debris-covered glaciers including heat conduction through the debris layer, J. Glaciol., 56, 903–916, 2010. 7522

RST: Radar Systemtechnik GmbH, available at: http://www.rst-group.biz (last access: 11 June 2012), 2012. 7511

Schaefli, B.: Quantification of modelling uncertainties in climate change impact studies on water ressources, Ph.D. thesis, EPFL-Lausanne, no. 3225, 2005. 7509

Schneeberger, C., Blatter, H., Abe-Ouchi, A., and Wild, M.: Modelling changes in the mass balance of glaciers of the northern hemisphere for a transient $2CO_2$ scenario, J. Hydrol., 282, 145–163, doi:10.1016/S0022-1694(03)00260-9, 2003. 7509

Schwarb, M., Daly, C., Frei, C., and Schär, C.: The mean annual and seasonal precipitation throughout the European Alps 1971–1990, Vol. 2-6–2-7, Hydrological Atlas of Switzerland, 2001. 7514

Singh, P. and Kumar, N.: Impact assessment of climate change on the hydrological response of snow and glacier melt runoff dominated Himalayan river, J. Hydrol., 193, 316–350, 1997. 7508, 7509

Stokes, C., Popovnin, V., Aleynikov, S., Gurney, S., and Shahgedanova, M.: Recent glacier retreat in the Caucasus Mountains, Russia, and associated increase in supraglacial debris cover and supra-/proglacial lake development, J. Glaciol., 55, 444–452, 2009. 7522

van der Linden, P. and Mitchell, J.: ENSEMBLES: Climate Change and its Impacts: Summery of research and results from the ENSEMBLES project, Met Office Hadley Centre, Exeter EX1 3PB, UK, 160 pp., 2009. 7514

VAW: Mauvoisin – Giétrogletscher – Corbassièregletscher. Glaziologische Studien im Zusammenhang mit den Stauanlagen Mauvoisin, im Auftrag der Elektrizitätsgesellschaft Lauffenburg AG, (M. Funk, unveröffentlicht), 1998. 7511

Vieli, A., Funk, M., and Blatter, H.: Griesgletscher: Berechnungen des Gletscherfliessens und Perspektiven für die Zukunft, Wasser Energie Luft, 89, 107–114, 1997. 7509

HESSD

9, 7507–7541, 2012

Ice volume distribution and implications on runoff projections

J. Gabbi et al.

Table 1. Area, ice volume, altitudinal range and main exposition of the glaciers in the Mauvoisin region. Data refer to 2009.

Glacier	Area km^2	Volume km^3	Alt. range m a.s.l.	Expo
Corbassière	18.26	1.379	2235–4315	N
Otemma	15.74	1.052	2465–3815	SW
Brenay	8.99	0.384	2575–3815	SW
Mont Durand	6.98	0.298	2360–4160	NE
Giétro	5.46	0.447	2620–3815	NW
Tsessette	3.05	0.076	2490–4025	E
Petit Combin	2.53	0.023	2665–3665	N
Fenêtre	0.67	0.014	2575–3150	NE
Crête Sèche	0.60	0.009	2645–3150	NE
Tournelon Blanc	0.39	0.004	3140–3690	E
Lire Rose	0.14	0.001	3095–3225	SW

HESSD
9, 7507–7541, 2012

Table 2. Availability of different data sets used for this study: mass balance measurements (MB), DEMs, and the length of GPR profiles. Numbers in brackets indicate the fraction of ground-based GPR profiles from the total length of helicopter- and ground-based GPR profiles for each galcier.

	MB	DEMs	GPR
Corbassière	1996–2009	1934, 1985, 1997, 2003, 2009	34 (9) km
Giétro	1966–2009	1934, 1983, 1998, 2003, 2009	17 (6) km
Brenay	–	1934, 1983, 2009	8 km
Otemma	–	1934, 1983, 2009	15 km
M. Durand	–	1934, 1983, 2009	8 km
small gl.	–	1934, 1983, 2009	–

HESSD

9, 7507–7541, 2012

Ice volume distribution and implications on runoff projections

J. Gabbi et al.

Table 3. Summary of the main results of this study. The evolution of the ice volume, the glacierized area, the annual runoff and the different runoff components (ice melt, snow melt, runoff from non-glacierized area and runoff from the subsurface) is shown for the period 1950–2100 in 30-yr steps.

Quantity	Unit	1920	1950	1980	2010	2040	2070	2100
Ice volume	km^3	6.2	5.3	4.3	2.4	1.8	0.6	0.1
Glacier area	km^2	75.9	72.7	71.7	61.6	38.6	15.5	4.2
Annual runoff	$10^6\ m^3\ a^{-1}$	207	258	223	260	270	231	206
- $Q_{glacier}$	$10^6\ m^3\ a^{-1}$	37	48	31	55	67	30	9
- Q_{snow}	$10^6\ m^3\ a^{-1}$	101	127	119	117	99	76	60
- $Q_{non\text{-}glacierized}$	$10^6\ m^3\ a^{-1}$	3	4	4	11	22	30	34
- $Q_{subsurface}$	$10^6\ m^3\ a^{-1}$	66	79	69	77	82	95	103

HESSD
9, 7507–7541, 2012

Ice volume distribution and implications on runoff projections

J. Gabbi et al.

Table 4. Area, maximal (H_{max}) and mean (H_{avg}) ice thickness, ice volume of (1) ($V_{(1)}$), ice volume of (5) ($V_{(5)}$), the relative ice volume difference between $V_{(1)}$ and $V_{(5)}$ ($V_{(5:1)}$), the calibrated apparent mass balance gradients for the ablation ($d\tilde{b}/dz_{abl}$) and accumulation zone ($d\tilde{b}/dz_{acc}$) and the calibrated correction factors (c) of the Mauvoisin region.

Glacier	Area [km^2]	H_{max} [m]	H_{avg} [m]	$V_{(1)}$ [km^3]	$V_{(5)}$ [km^3]	$V_{(5:1)}$ [%]	$d\tilde{b}/dz_{abl}$ [10^{-2} a^{-1}]	$d\tilde{b}/dz_{acc}$ [10^{-2} a^{-1}]	c [–]
Corbassière	18.3	238	76	1.38 ± 0.07	1.96	+42	0.55	0.14	0.707
Otemma	15.7	291	67	1.05 ± 0.05	1.42	+35	0.68	0.27	0.755
Brenay	9.0	212	43	0.38 ± 0.02	0.61	+61	0.66	0.38	1.040
Mont Durand	7.0	144	43	0.30 ± 0.02	0.54	+80	0.59	0.65	1.355
Giétro	5.5	230	82	0.45 ± 0.02	0.42	−7	0.81	0.70	0.542
small glaciers	7.3	83	19	0.13 ± 0.05	0.08	−38	0.66	0.43	0.873
Mauvoisin	62.8	291	59	3.69 ± 0.11	5.03	+36	0.66	0.43	0.873

HESSD
9, 7507–7541, 2012

Title Page
Abstract Introduction
Conclusions References
Tables Figures
◂ ▸
Back Close
Full Screen / Esc
Printer-friendly Version
Interactive Discussion

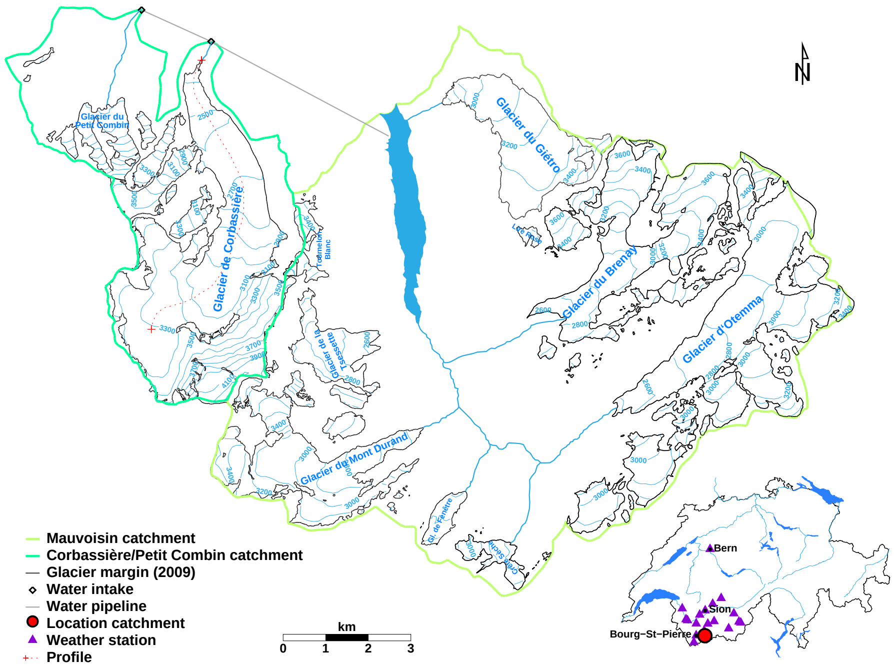

Fig. 1. Overview of the Mauvoisin region. The inset on the bottom left shows the location of the catchment and the weather stations used in this study. The red dashed line refer to the profile of Fig. 9.

HESSD

9, 7507–7541, 2012

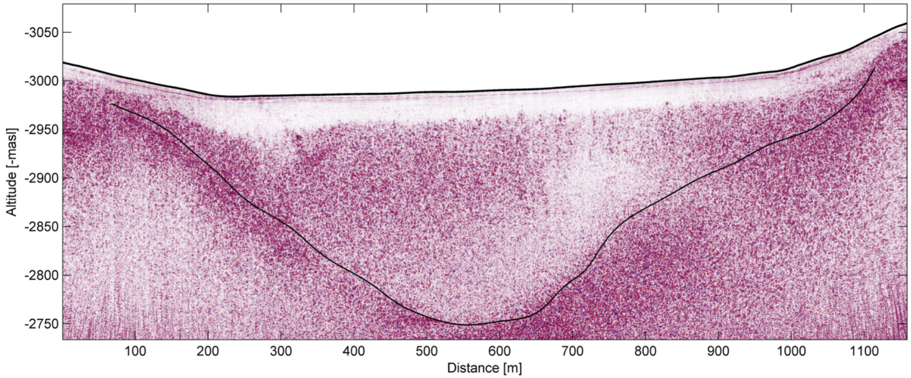

Fig. 2. Processed GPR section across Glacier d'Otemma. Its position is indicated in Fig. 3.

HESSD

9, 7507–7541, 2012

Ice volume distribution and implications on runoff projections

J. Gabbi et al.

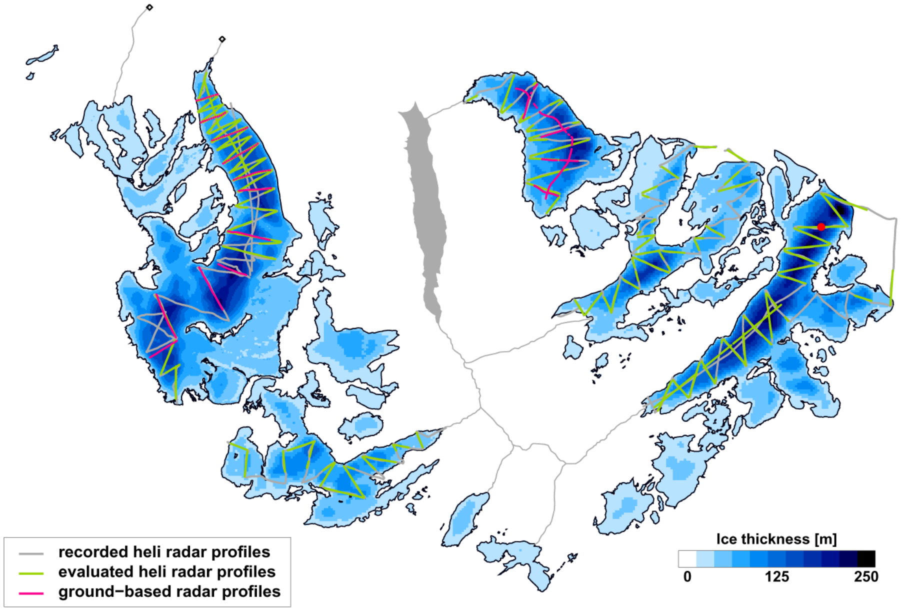

Fig. 3. Ice-thickness distribution in the Mauvoisin region derived by all available ice-thickness measurements. Glacier outlines refer to 2009. The grey lines show the recorded helicopter-based GPR profiles, the green lines the finally evaluated profiles and the red lines the ground-based GPR profiles from previous field campaigns. The red dot refers to the GPR section shown in Fig. 2.

HESSD
9, 7507–7541, 2012

Ice volume distribution and implications on runoff projections

J. Gabbi et al.

Title Page
Abstract Introduction
Conclusions References
Tables Figures
◀ ▶
Back Close
Full Screen / Esc
Printer-friendly Version
Interactive Discussion

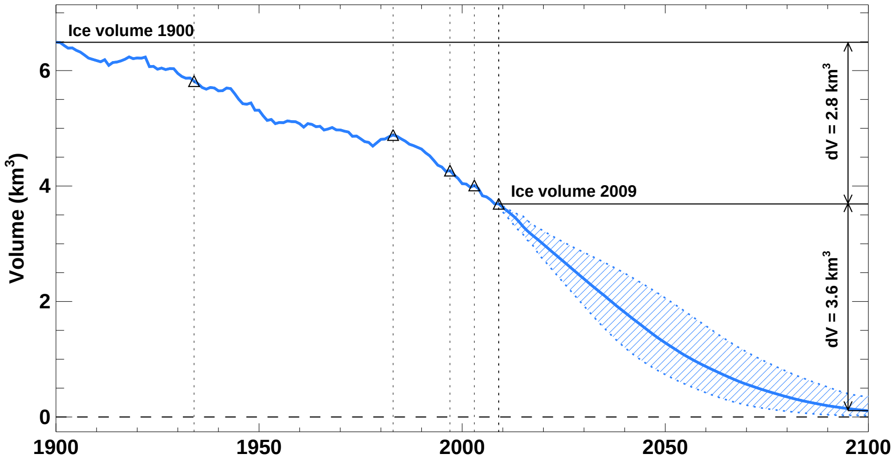

Fig. 4. Ice volume evolution in the Mauvoisin region between 1900 and 2100. The hatched zone represents the 95 % confidence interval of the multiple model runs. Black triangles and corresponding dotted lines show years in which a DEM was available.

HESSD
9, 7507–7541, 2012

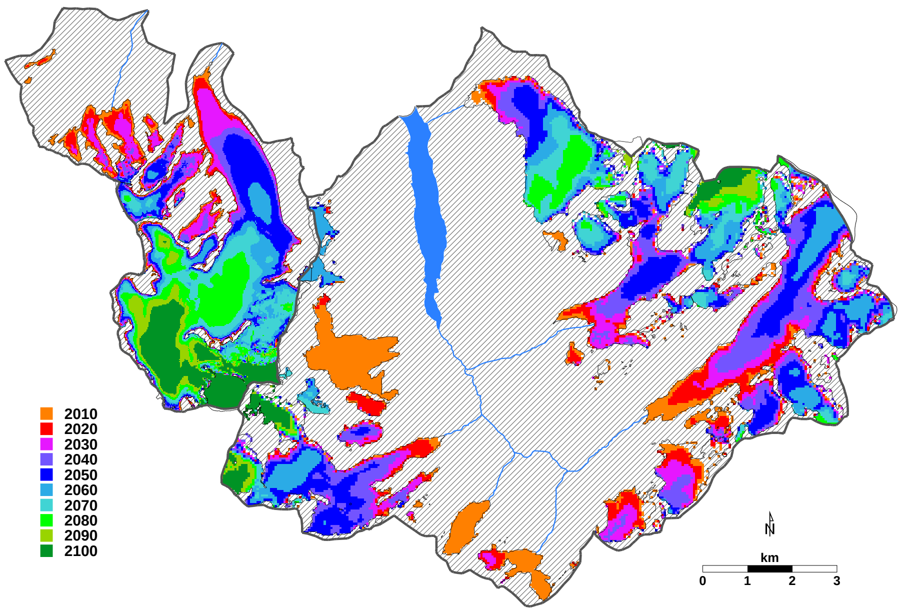

Fig. 5. Projected glacier retreat in the Mauvoisin region until the end of the 21st century. Glacier area is shown in 10-yr steps. Hatched zones framed by the gray thick lines represent the outlines of the two subcatchments Mauvoisin and Corbassière/Petit Combin.

HESSD
9, 7507–7541, 2012

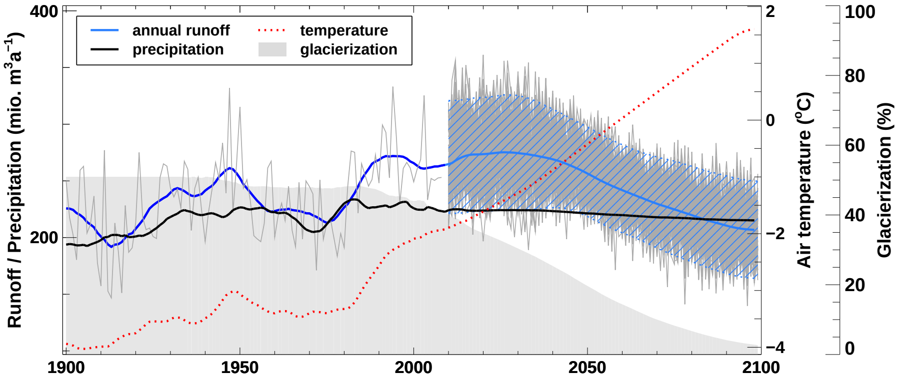

Fig. 6. Evolution of annual runoff volume, precipitation, air temperature and glacierization in the Mauvoisin catchment. Bold lines represent running means, thin gray line the effective evolution of the annual runoff. The hatched zone indicates the 95 % confidence interval of the annual runoff determined from multiple model runs. The gray shaded area refers the percentage of ice covered area in the catchment.

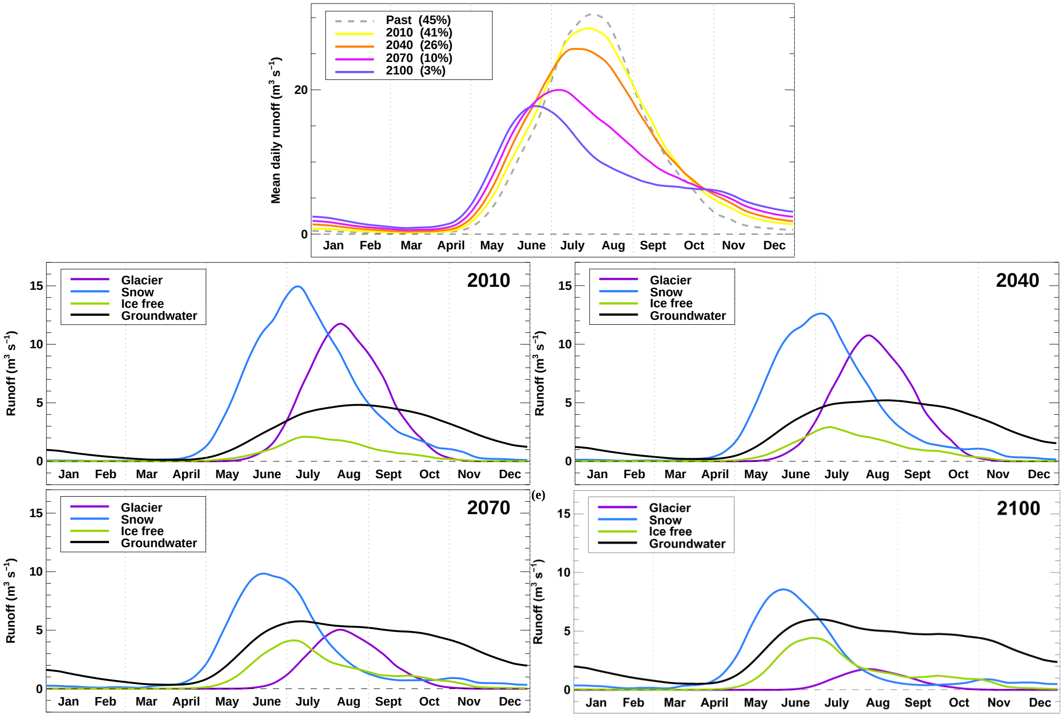

Fig. 7. Evolution of the runoff regime in the Mauvoisin region for the reference period and four time snapshots in the future avreaged over ±5 yr (top). Numbers in brackets refer to the percentage of glacier cover. The lower four figures show the evolution of the runoff components for the same time points in future.

HESSD
9, 7507–7541, 2012

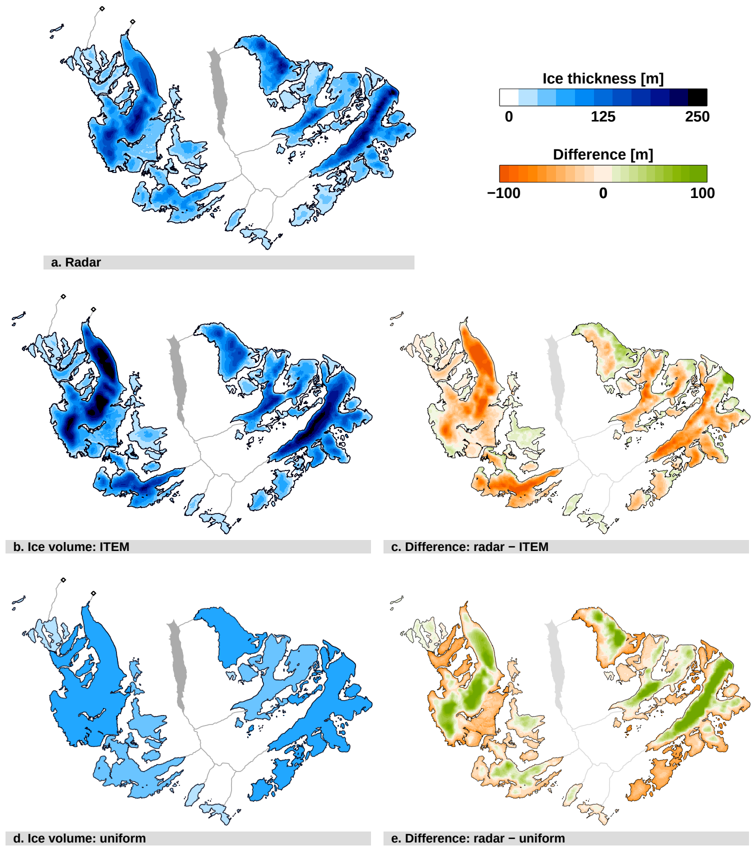

Fig. 8. The different ice-thickness distributions: **(a)** the GPR based ice volume distribution, **(b)** the ice-thickness distribution derived by ITEM and **(d)** uniform ice-thickness distribution. The figures on the right side **(c, e)** refer to the ice thickness difference to the reference distribution determined by measurements.

HESSD
9, 7507–7541, 2012

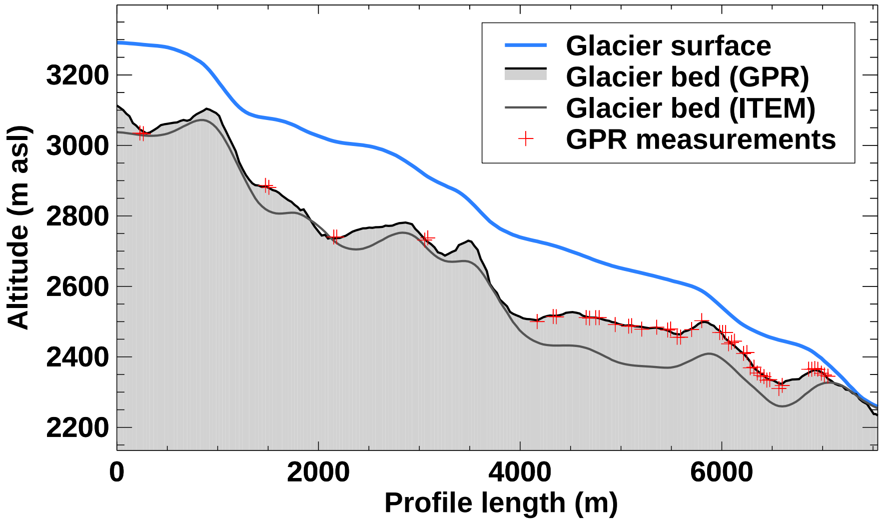

Fig. 9. Longitudinal profile along the central flow line of the Glacier de Corbassière (see Fig. 1). The thin black line refers to the glacier bed derived by the GPR measurements, the thin gray line to the bed computed by the ITEM and the blue line to the glacier surface. The red crosses mark the GPR based ice-thickness measurements

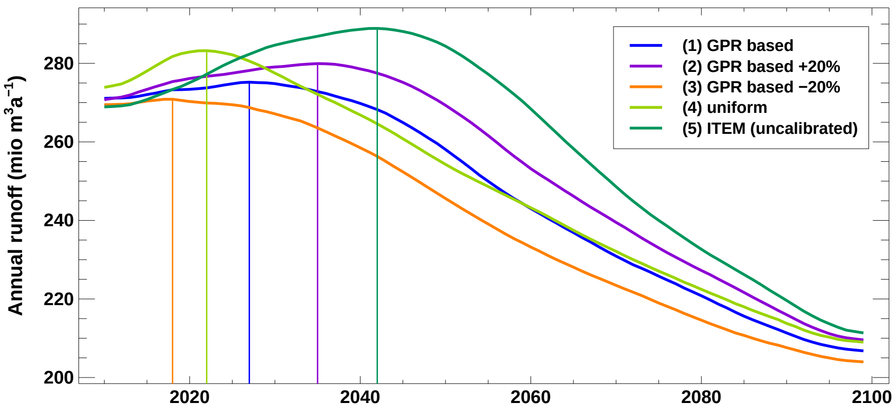

Fig. 10. Runoff projections based on the different initial ice-thickness distributions. The numbers in brackets refer to the list of the different tested initial ice volume distribution in Chapter 5.

HESSD
9, 7507–7541, 2012